Revealing the noctilucent cloud fields structure by software processing of satellite images

A.A. Solodovnik [ID] , R.A. Kleksin [ID] , P.I. Leontyev [ID] ,

B.M. Useinov* [ID] , A.G. Markova [ID] and S.A. Kassimova [ID]

M. Kozybayev North Kazakhstan University, Petropavlovsk, Kazakhstan
*e-mail: buseinov@gmail.com

Noctilucent clouds, which form during the summer months primarily over the polar regions, are also frequently observed at temperate latitudes. These regions play a key role in shaping the total area and spatial configuration of mesospheric cloud fields. As shown in previous studies, the seasonal and interseasonal evolution of these fields is largely influenced by meteorological processes in the mesosphere, though the role of geophysical fields is also considered. This work describes the development of a methodology that enables a shift from studying the integral characteristics of noctilucent clouds to analyzing their differential properties. At the initial stage, the goal is to investigate the presence of longitudinal structure by dividing satellite images of noctilucent cloud fields into 30-degree longitudinal sectors and calculating the cloud area within each. Achieving this requires the creation of specialized software, and a significant portion of the study is devoted to describing the algorithm design, programming language selection, and implementation process. The performance of the new software is compared with existing approaches, demonstrating that the developed method provides substantially improved accuracy in detecting longitudinal inhomogeneities in the global distribution of noctilucent clouds.

Key words: noctilucent clouds, digital images, longitudinal cloud structure, hydrometeorology, hydroclimatology, cloud physics and chemistry.
PACS number(s): 92.60.H-; 96.12. Jt; 95.85.-e.

1 Introduction

Although noctilucent clouds (NLC are studied across several scientific disciplines, they are of particular interest to astronomy and geophysics. This interest was initially sparked by their discovery and has since grown, especially in the context of atmospheric physics and comparative planetology.

These cloud formations are located in the mesosphere at altitudes of about 80 km, where moisture levels are extremely low, making them largely irrelevant for traditional meteorological studies. At the same time, the seasonality of their appearance, associated with a change in the nature of atmospheric circulation, the effectiveness of the influence of cosmic factors on the highest layers of the atmosphere and, finally, the presence of similar cloud formations in the atmospheres of other planets, are attractive to specialists in the field of upper atmosphere physics, climatology, planetology [1-4].

The unique conditions for observing NLC in the twilight sky and the seasonality of their appearance determined the methods for studying these objects. Their high-altitude location makes conventional meteorological tools such as balloon or aerial sounding ineffective. As a result, most scientific data on NLCs have been obtained through remote sensing techniques, including both ground-based and satellite observations. Space-based monitoring, unaffected by weather conditions, offers a far greater volume of data than ground-based methods. One of the most successful missions for investigating the nature of NLCs has been the operation of the AIM (Aeronomy of Ice in the Mesosphere) satellite [5]. Many of the measurement results collected during this mission are publicly available and provide valuable insights into the genesis and evolution of noctilucent clouds.

In our study, the objective was to investigate the spatial structure of global noctilucent cloud (NLC) fields, with a particular focus on determining whether

these cloud formations exhibit longitudinal symmetry or contain significant inhomogeneities.

2 The influence of meteorological factors on the state of noctilucent clouds fields

By now, there is a fairly accurate picture of the seasonal occurrence description of the mesospheric cloud fields. This picture is based on the change in the nature of atmospheric circulation at the heights of the mesosphere and stratosphere during the «winter-summer» transition. The main role is played by the ascending flows of air masses, leading to a significant decrease in temperatures in the upper part of the mesosphere in summer. In this case, water vapor in the mesosphere becomes supersaturated and condensation occurs. Taking into account the fact that these processes are characteristic for subpolar latitudes, the annual formation of the polar mesospheric clouds "caps" in the summer seasons should be associated with them [6 – 8].

However, in the summer seasons, NLC are also observed in temperate latitudes. It is not at all necessary that their appearance is associated only with the drift (advection) of mesospheric cloud formations in the meridional direction. The appearance of NLC in temperate latitudes is also explained by the influence on the temperature regime of the mesosphere of internal gravity waves (IGW) – density waves propagating in horizontal and vertical directions. An adiabatic decrease in the temperature of the mesosphere at the crests of such waves contributes to the condensation of water vapor and the formation of high-altitude clouds [9 – 11].

The source of IGW can be various processes associated with large-scale energy release, but most likely they owe their origin to meteorological processes in the troposphere – the movement of atmospheric vortices and fronts, occlusions, orographic effects. Currently, the study of the influence of IGW on the genesis and evolution of NLC fields reveals its high relevance [12].

Of course, considering the evolution of NLC fields, it is impossible to exclude from consideration the influence of the water vapor inflow processes into the mesosphere. But general research in this direction is hampered by the lack of accurate data on the content of water vapor both at different height levels and at different latitudes and longitudes in the upper atmosphere.

Recent (2018) studies [13-14] show that NLC fields may be associated with climate change, and, specifically, with an increase in the amount of green-house gases in the atmosphere. Large-scale atmospheric processes, such as increases in ocean surface temperatures or changes in air circulation patterns, can lead to changes in the distribution and intensity of NLC. The results of research in this area are quite unexpected and clearly demonstrate the lack of the process and consequences understanding of climate change in the last few centuries, creating another relevant area for research.

Thus, large-scale atmospheric processes play a significant role in the formation and development of NLC fields. Research in this area helps to better understand atmospheric interactions and their influence on climate processes. However, to conduct such research it is necessary to obtain data in a convenient for study format (mainly comparative). To obtain such data, we can use the method of synthetic mapping. This method is based on the analysis of data obtained from spacecraft and allows you to create maps that reflect the distribution of NLC at various latitudes and longitudes. This method also makes it possible to more accurately monitor changes in cloud distribution dynamics and identify possible trends.

Synthetic map is a map that provides an integral image of an object or phenomenon in unified synthetic indicators [15]. In our case, synthetic maps are a combination of photographic observations along a separate orbit of the spacecraft as shown in figure 3.

3 Methods for studying tropospheric-mesospheric relations

The methodology of studying the influence of tropospheric processes on the evolution of NLC in temperate latitudes has proved to be extremely productive. This approach is based on a cartographic analysis of data on the daily dynamics of NLC in the northern hemisphere, correlated to the maximum extent with data on meteorological phenomena occurring at the same time [16-19]. When constructing images of the NLC field, data from the AIM mission was used [5], while meteorological information was received from relevant sources. The analysis of such maps has shown that in most cases there is a relation between the nature of the meteorological events development in the troposphere and the formation of the NLC field features. The main factors influencing mesospheric processes are the following: the movement of cyclones in the zonal direction with the intersection of the Ural Mountains, the meridional (from north to south) movement of cyclones, the development of occlusions and thunderstorm foci, as well as the oncoming movement of atmospheric fronts.

These processes are effective sources of density waves (IGW) that reach the mesosphere and influence the temperature regime at significant heights.
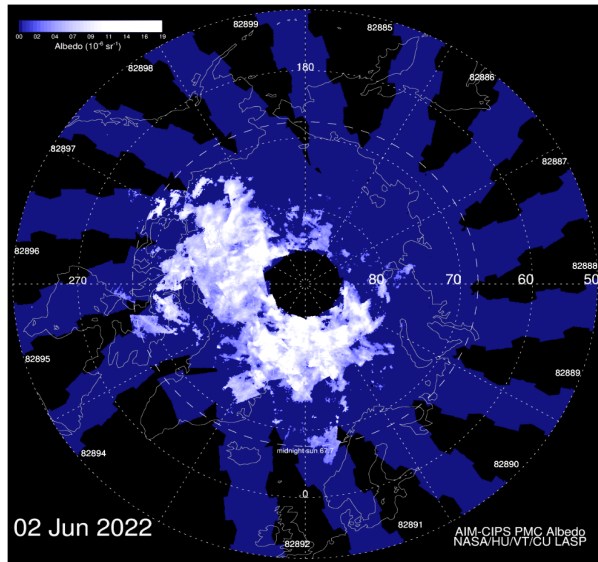

Figure 1 – Synthetic map of noctilucent cloud fields
in the northern hemisphere
obtained by the AIM satellite.

On the other hand, the analysis of the tropospheric processes effect on NLC generation included a study of the temperature regime effect in Antarctica on the formation of mesospheric clouds in the southern hemisphere. In this context, high correlations were found between temperature changes in the South Pole region and changes in the total area of the NLC field [20]. A special feature here is the detected characteristic time lag between these two parameters, the graph showing this correlation is given in figure 2 [14].

Shown results are surface area of the noctilucent clouds for the southern hemisphere (red) and average daily temperatures of the South Pole (blue) for two seasons. Here it is important to note the climatic feature of Antarctica, where temperature changes in the pole region essentially reflect changes in the average temperature for the entire continent. When studying the relationship between temperature changes and changes in the area of the NLC field in the North Pole region, it is necessary to move from determining the general characteristics of the NLC field to a differential representation, that is, to studying the longitude distribution of mesospheric clouds. But this requires the development of a new software package and processing of a large array of images with its help.
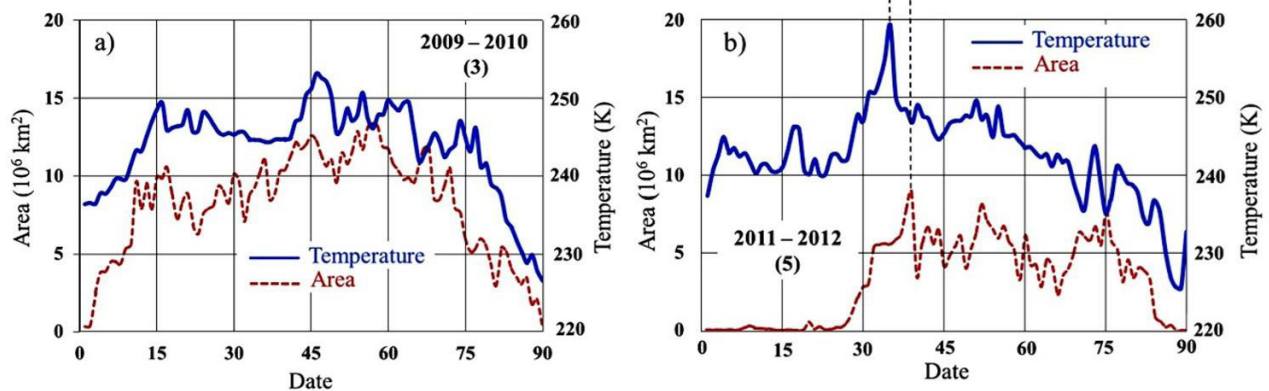

Figure 2 – Seasonal changes in the NLC field area.

4 Structure and algorithm of the satellite image processing program

To develop the program, the high-level, object-oriented, multi-paradigm programming language *Python* was chosen. In the context of the problem being solved, its main advantage was its modularity, which allows, using the simplest commands within the en-

vironment and the compiler, to integrate specialized code libraries into the created program. The free *PyCharm Community Edition*, which has a large list of tips and built-in documentation for the language, was used as a compiler. The development environment is made virtual using the *Anaconda* distribution for ease of handling libraries. The program must meet the following requirements: the ability to work

with an entire array at once, dividing each image in the array into 12 sectors of 30 degrees, calculating the area of the NLC in each of them and saving the result in an Excel table. This functionality allows you to reduce the time for obtaining data necessary for analyzing the development of an object.

Each image is accompanied by a file with data encoded in it, including the area in each pixel. This is necessary to convert the results of the program. The document file is in IDL dataset format. To extract this data, you will need a separate IDL reader program. Since the data of the entire dataset is not needed, it is advisable to create a compact version of the IDL reader that reads only the indicator that interests us. In figure 3 the code of such reader is presented.

```
1   from netCOF4 import Dataset
2
3   # Specify the data array
4   nc_file = Dataset('cips_sci_3a_2020-153_v05.20_r05.nc', 'r')
5   # Specify the required variable
6   data_varlablel = nc_flie.variables['KM_PER_PIXEL'][:]
7   # Output the result to the compiler console
8   print("km per pixel", data_varlablel)
9   # Close file
10  nc_file.close()
```

Figure 3 – Algorithm for converting cloud image elements into
the format required for software processing.

If necessary, you can always increase the number of variables extracted from the array at a time by adding *Python* variables: *data_variable2, data_variable3, data_variable4*, etc. After that, having received the names of the necessary variables from the AIM website (or another source), to indicate for each the correspondence with the contents of the array. If you use the latest version of the data (they are always available), the desired variable does not change, and you can then use it in all calculations.

To check the effectiveness of the developed software package, a control image was created and is shown in figure 4, the required information on which is easily accessible for direct calculation.

The image is represented by a background on which a white square of 100 by 100 pixels is placed. The area of this object is precisely calculated: 10,000 pixels are multiplied by 7.5 sq. km/pixel, which gives a result of 75 thousand sq. km. To eliminate the influence of the background, a complex method was chosen: a combination of threshold filtering, background subtraction and zones of interest.
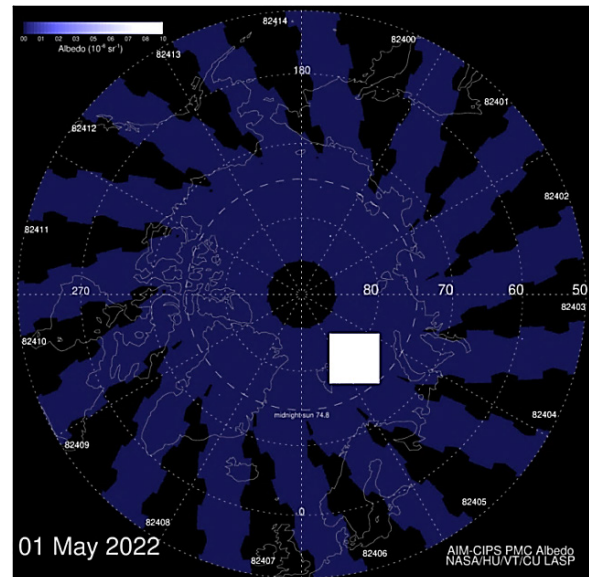

Figure 4 – An image of the circumpolar region with a
background. The area is highlighted
with a square to control the accuracy.

5 Description of the algorithm and logic of individual solutions

To perform the assigned tasks, specialized libraries were selected and are listed below.

OpenCV (cv2): used for reading, processing and analyzing images using a wide range of methods.

NumPy: used for introducing advanced mathematical operations and working with arrays into code.

- *Pandas*: provides data structuring and tools for their analysis. Responsible for exporting to Excel.

- *Tkinter*: serves to create a graphical interface allowing the user to select directories.

- *MatPlotLib*: allows you to demonstrate *cv2* and *numpy* operations; it was used for calibration and adjustment.

- *Os*: a helper library used to interact with a computer's file system.

Then the program algorithm was set up, as shown further.

1. Setting up GUI for directory selection: *Tkinter* is used to create an interface through which the user can select a directory of images for analysis.

2. Reading the image: using *OpenCV*, the program reads images from the selected directory, then *os* indexes and sorts them.

3. Binarization: OpenCV converts images into matrix form and applies threshold filtering.

4. Background subtraction: the absolute difference between the "background" matrix and the target image matrix is calculated.

5. Creating masks: a mask is created that completely covers the image with zero pixels, then a mask is created in the shape of a circle of a certain radius. Inside this mask, based on the angular geometry, masks of individual sectors are created, which in turn cancel the "shading" effect and allow the calculation algorithm to operate within its geometry.

6. Calculation of the sectors area: the number of pixels not covered by "shading" masks is counted and the area covered by the sector is calculated, converting the number of pixels into square kilometers.

7. Saving results: The results of sector area analysis are saved to an Excel file. After which cycle 2-6 is repeated until all images have been processed.

Two functions stand out in the general code. The *«slice_mask»* function accepts image and sector parameters, creating a mask to highlight the area of a particular sector. This is achieved by drawing lines and arcs that define the inner and outer boundaries of the sector. The areas of the image that lie outside the boundaries of the sectors are filled with zeros and excluded from the calculation. The *«calculate_sector_areas»* function applies a background subtraction algorithm, converts the image to binary format and uses masks created by the first function to determine the area of each sector [22].

Two program blocks are responsible for determining the initial and final sectors and working with angles in the program, one block for each function. For example, the block shown in Figure 5 is responsible for working with angles.

```
sector_areas = np.zeros(12)
for i in range(12):
    start_angle = 90 – (i + 1) * 30    # Start sector angle
    end_angle = 90 – (i) * 30          # End sector angle

    # Creation the sector mask
    sector_mask = slice_mask(image,center,inner_radius,outer_radius,start_angle,end_angle)
```

Figure 5 – Algorithm for selecting a longitudinal sector in processed images.

In mathematical expression, the point search algorithm looks like this:

$$x = \left(c[0] + r \cdot \cos(\alpha)\right), \quad y = \left(c[1] + r \cdot \sin(\alpha)\right) \quad (1)$$

where x is a point, c is the center (0 and 1 mean the axes, for each of which the center is determined separately), r is the radius, α is the angle, which is determined by the block shown in Figure 5.

Before data can be stored in Excel, it is collected and organized according to a format that is most readable and easy to analyze [24]. To organize the results of sector area measurements, the *DataFrame* method from the *Pandas* library is used. Each row of the *DataFrame* corresponds to one image, and the columns represent individual sectors. The program goes through all the images in the selected directory, analyzes them and fills the *DataFrame* with the received data. To save the *DataFrame* in Excel, the *to_excel* method is used, which is part of the *Pandas* library. This method specifies the path to the file where the data will be saved and the label for the index (index_label='Image'), which provides the addition of descriptive headers for rows in an Excel file.

As a result of executing the algorithm, the user, after a few seconds (depending on the size of the directory), receives an Excel file convenient for analysis with accurate and systematized data on the areas of the analyzed images sectors. For example, Table 1 shows data for two images: a test image and one working image, for June 1, 2020. The cells of the table show the sector areas for the conditional image (Figure 4) and the NLC fields (Figure 1), calculated in square kilometers, according to the described method. For the test image (Figure 4), a nominal value of 75 thousand km^2 is known.

Table 1 – Results of image processing shown in Figures 4 and 1.

	Sectors													
	1	2	3	4	5	6	7	8	9	10	11	12	Calc.	Nom.
Fig. 4	14775	60135	1103	0	0	0	0	0	0	0	0	0	76013	75000
Fig. 1	102975	61605	27645	9960	4553	21255	20243	131152	122888	107295	71505	107505	-	-

We can compare this value with the calculated sum of indicators for all sectors obtained during the program: 76 thousand km^2. The observed error of 1 thousand km^2 (1.3%) can be caused by background dispersion when changing images as shown in figure 6. It is also possible that the error is partially caused by the shot effect, which is characteristic of any discrete objects. The error varies depending on the threshold filtering parameter, but if this parameter is too high, there is a risk of data loss.
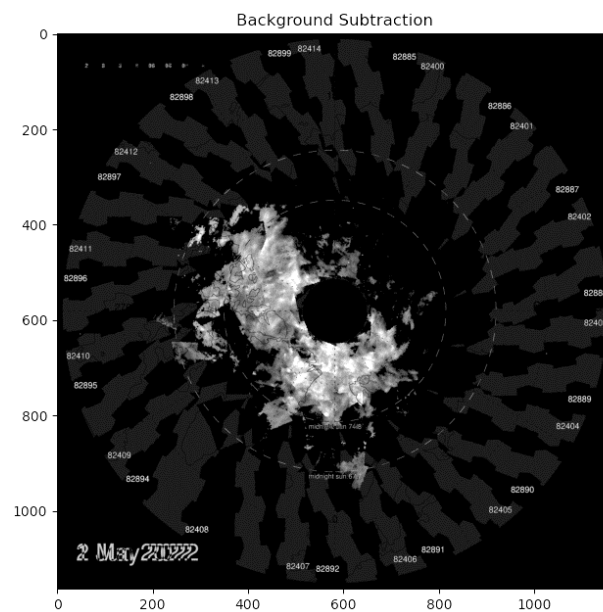

Figure 6 – View of the global noctilucent cloud field
after removing the background influence.

6 Some results of image processing of mesospheric cloud fields

Naturally, the main indicator of the practical value of the program can only be the results of processing satellite images of global NLC fields. In our case, we are talking about the seasons of their evolution from 2007 to 2022 (excluding the 2018 season). The lack of data on the AIM mission website for the 2018 summer season is due to technical reasons.

Table 2 – Final data on the distribution of the cloud fields area.

		Sectors											
		1	2	3	4	5	6	7	8	9	10	11	12
Seasons	2007	122601	124411	126350	124846	*121474*	129181	128701	**137061**	128037	122211	130344	**135432**
	2008	128283	120842	117123	118101	113286	117337	128473	118477	*111245*	*111287*	112750	**135556**
	2009	113429	113032	114379	*105623*	*106856*	119411	125047	124442	115057	108336	117975	**135387**
	2010	123277	126652	123245	118194	*113971*	126455	126258	**130122**	118444	*113009*	119484	**130812**
	2011	137475	136082	139701	138750	127739	131639	**144846**	143298	129263	*115371*	125453	**149688**
	2012	**132468**	123818	116832	121792	120925	124937	126614	124328	114381	*112243*	*112557*	**132203**
	2013	133645	123876	127421	127109	125155	133381	141900	137145	124888	*122010*	127701	**146562**
	2014	110886	104807	112024	108717	*102969*	*102125*	114820	115719	*102782*	104463	105302	**119809**
	2015	**144096**	133663	128889	*119840*	120822	127821	**140253**	138878	127618	124345	*120545*	137663
	2016	115647	98901	100761	100280	106067	105318	110933	**119256**	94661	96254	*88684*	100782
	2017	116102	110429	110199	104461	*101964*	107566	123241	**125878**	106725	113296	111475	106830
	2019	124333	124859	123104	118423	112784	*111894*	125015	**131895**	122845	113811	126065	121269
	2020	128248	134339	130372	123670	123854	127481	128995	**146412**	122379	*112798*	132670	132079
	2021	123580	126311	121126	121557	119537	122826	128685	**135952**	119991	*115836*	127007	124207
	2022	116016	116254	120530	114892	107116	113135	117100	**122985**	112432	*110530*	118948	**126343**
	Aver.	124672	121218	120804	117750	114968	120034	127392	130123	116716	113053	118464	128975
	Norm.	1,029	1,000	0,997	0,972	0,949	0,991	1,051	1,074	0,963	0,932	0,979	1,064

In each season, 90 daily pictures were included in the processing, that is, the total number of images studied was about 1350. In this case, the time required was no more than 10 hours. The final data on the distribution of the cloud fields area, expressed in square kilometers, for 12 longitudinal sectors on average per season are presented in Table 2.

The last lines show the average cloud area for all seasons (second line from the bottom) and the same values normalized to the average cloud area in all sectors and for all seasons. Cells corresponding to the maximum cloud field areas in the sector for a given season are highlighted in bold (differences of 1-2% are considered acceptable). Sectors with the minimum area of the cloud field are highlighted in italics and gray shading.

The table data indicates the existence of stable trends, that is, sectors with a predominance of maximum or minimum areas of cloud fields in relation to the average in the sectors. This fact is clearly illustrated in Figure 7, where the differences in the longitudinal structure are shown in the form of a bar graph.
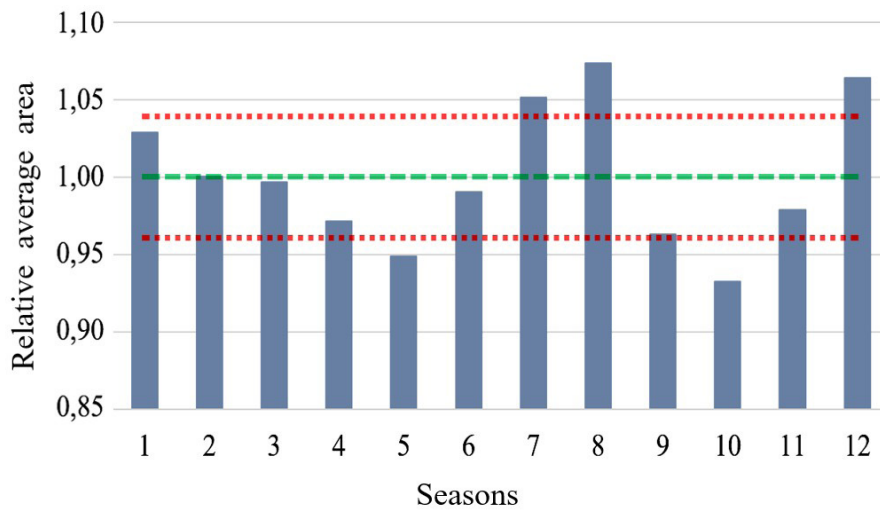
Figure 7 – Distribution of normalized average field area values
NLC in the northern hemisphere by longitudinal sectors for all seasons.

It should be noted that Figure 7 shows both the average value of the relative area of the cloud field and the maximum deviations of these values, corresponding to a confidence level of 98% (plus or minus triple the root mean square error of the average value). Thus, we can confidently speak about the existence of stable maxima in the development of the cloud field in sectors 7, 8 and 12. At the same time, minimal development of the area of NLC fields is typical for sectors 5 and 10. These facts, in our opinion, deserve further study as it can lead to discovery of new NLC relations with geophysical events or phenomena.

7 Conclusion

The developed program is a convenient tool for analyzing longitudinal variations of NLC fields, being a reliable foundation in studies of the connection between various physical processes and the evolution of NLC. The program not only provides accurate data, but also allows you to automate routine image processing, which speeds up data analysis and improves its quality.

Acceptable accuracy has been achieved when processing working arrays. Distortions in the result caused by background dispersion create an insignificant error and, in the future, can be eliminated using machine learning algorithms or background subtraction methods. The structure of the program and its development environment are flexible enough to allow modification in the future. As an advantage over analogues, we can highlight the fact that the version from the current work, if necessary, can be provided with an executive file and a compact directory with the necessary libraries, which will allow it to be used with a minimum of presets.

Using the created program, a general analysis of the satellite images array of the northern hemisphere global NLC field was carried out over a long period of time. The results obtained reliably indicate the presence of longitude sectors with statistically significant differences in the development of mesospheric clouds. This suggests the need to continue research in this direction.

References

1. Gadsden, M., and Schroder W. Noctilucent Clouds. – New York: Springer – 1989. – P. 125-130.
2. Grishin, N.I. Studies of Mesospheric Clouds. // In Proceedings of Meteorological Studies. Physics of the Mesosphere and Mesospheric Clouds, edited by O.B. Vasyl'ev. – Moscow: Nauka – 1975. – P. 23–32. (In Russian)
3. Bronshten, V.A., Grishin N.I. Noctilucent Clouds. – Moscow: Nauka – 1970. – 359 p. (In Russian)
4. Turco, R.P., Toon O.B., Whitten R.C., Keesee R.G., Hollenbach D. Noctilucent Clouds: Simulation Studies of Their Genesis, Properties, and Global Influences. // Planetary and Space Science 30. – 1982. – no. 11 P. 1147–1181.
5. Aim Mission Overview. AIM. Exploring Clouds at the Edge of Space. http://aim.hamptonu.edu/mission/index.html (accessed May 27, 2025).
6. Olivero J.J., Thomas G.E. Climatology of polar mesospheric clouds // Journal of the Atmospheric Sciences 43. – 1986. – no. 12 – P. 1263–1274.
7. Berger U., Lübken F.-J. Trends in mesospheric ice layers in the northern hemisphere during 1961–2013 // Journal of Geophysical Research: Atmospheres 120. – 2015. – P. 11.277–11.298. https://doi.org/10.1002/2015JD023355
8. Thurairajah B., Cullens C.Y., Bailey S.M. Characteristics of a mesospheric front observed in polar mesospheric cloud fields // Journal of Atmospheric and Solar-Terrestrial Physics. – 2021. -P. -Vol. 208. – Art. 105627. https://doi.org/10.1016/j.jastp.2021.105627
9. Shevchuk N., Pertsev N., Dalin P., Perminov V. Wave-induced variations in noctilucent cloud brightness: Model and experimental studies // Journal of Atmospheric and Solar-Terrestrial Physics. – 2020. -P. Vol. 203. – Art. 105257. https://doi.org/10.1016/j.jastp.2020.105257
10. Chandran A., Rusch D.W., Thomas G.E., Palo S.E., Baumgarten G., Jensen E.J., Merkel A.W. Atmospheric gravity wave effects on polar mesospheric clouds: A comparison of numerical simulations from CARMA 2D with AIM observations // Journal of Geophysical Research. – 2012. -Vol. 117. – Art. D20104. https://doi.org/10.1029/2012JD017794
11. Dalin P., Gavrilov N., Pertsev N., Perminov V., Pogoreltsev A., Shevchuk N., Dubietis A., Völger P., Zalcik M., Ling A., Kulikov S., Zadorozhny A., Salakhutdinov G., Grigoryeva I. A case study of long gravity wave crests in noctilucent clouds and their origin in the upper tropospheric jet stream // Journal of Geophysical Research: Atmospheres. – 2016. -Vol. 121. – No. 23. -P. 14.102-14.116. https://doi.org/10.1002/2016JD025422
12. DeLand M.T., Shettle E.P., Thomas G.E., Olivero J.J. A quarter-century of satellite polar mesospheric cloud observations // Journal of Atmospheric and Solar-Terrestrial Physics. – 2006. P. -Vol. 68. -P. 9–29. https://doi.org/10.1016/j.jastp.2005.08.003
13. Gao H., Li L., Bu L., Zhang Q., Tang Y., Wang Z. Effect of small-scale gravity waves on polar mesospheric clouds observed from CIPS/AIM // Journal of Geophysical Research: Space Physics. – 2018. -Vol. 123. – P. 4026–4045. https://doi.org/10.1029/2017JA024855
14. Shitikov V.K., Rosenberg G.S., Kostina N.V. Metody sinteticheskogo kartografirovaniya territorii (Na primere ekologo-informacionnoi sistemy «Region-Volgabas») https://ecograde.bio.msu.ru/library/books/_pdf_rozenberg/3-2.pdf (accessed May 27, 2025). (In Russian)
15. Solodovnik, A. A., Leontyev P. I., Dalin P. Studies of the influence of tropospheric factors on the formation of noctilucent clouds by a cartographic method // Journal of Atmospheric and Solar-Terrestrial Physics. – 2020. -Vol. 200. – Art. 105224. https://doi.org/10.1016/j.jastp.2020.105224
16. Kudabaeva D.A., Solodovnik A.A. Variation in the area of the global field of noctilucent clouds of the northern hemisphere in 2007–2012 seasons // Geomagnetism and Aeronomy. – 2015. -Vol. 55. -No. 2. – P. 261–265. https://doi.org/10.1134/S0016793215020139
17. Solodovnik, A., Baibusinova A., Kudabaeva D. Dynamics of the development of the field of noctilucent clouds in the northern hemisphere in the period 2013–2020 // Bulletin of KazNTU. – 2020a.- -Vol. 4. -No. 140. – P. 138–144.
18. Solodovnik, A.A., Baibusinova A.K. Features of the seasonal development of the fields of noctilucent clouds of the northern and southern hemispheres of the Earth // Eurasian Union of Scientists (EUS) 5. – 2020b. – No. 74. – P. 10–16.
19. Solodovnik A., Leontiev P., Dalin P., Takenov B., Alyoshin D. Seasonal evolution and interseasonal changes in polar mesospheric clouds at high latitudes in the southern hemisphere // Journal of Atmospheric and Solar-Terrestrial Physics. – 2021. -Vol. 226. – Art. 105787. https://doi.org/10.1016/j.jastp.2021.105787
20. Cole A. E., Kantor A. J. Air force reference atmospheres. – Hanscom AFB, Massachusetts: Air Force Geophysics Laboratory, Air Force Systems Command, United States Air Force. – 1978. – P. 76.
21. Bradski G., Kaehler A. Learning OpenCV: Computer vision with the OpenCV library. – O'Reilly Media. – 2008. -P. 577.
22. McKinney W. Python for data analysis. – O'Reilly Media. – 2012. – P. 541.
23. Langtangen, H. P. A primer on scientific programming with Python. – Springer. – 2016. – P. 716.
24. Summerfield M. Programming in Python 3: A Complete introduction to the Python language. – Addison-Wesley. – 2015. – 636 p.
25. Solodovnik A.A., Zyryanov R.O, Leontyev P.I., Useinov B.M., Gololobova E.G., Zhuravlev P.L. Experience of noctilucent clouds registering in the near infrared spectrum region // Physical Sciences and Technology. – 2024. – Vol. 11 (No. 1-2). – P. 85-93. https://doi.org/10.26577/phst2024v11i1a10
26. Solodovnik A.A., Leontyev P.I., Useinov B.M., Kadyrmin A.D., Zyryanov R.O. Application of electronic receivers for recording infrared images of celestial phenomena at the CAR of the NKU // Physical Sciences and Technology. – 2023. – Vol. 10 (No. 1-2). -P. 50-57. https://doi.org/10.26577/phst.2023.v10.i1.07

Information about authors:

Solodovnik Andrey, Candidate of Physico-Mathematical Sciences is a Professor at the M. Kozybayev North Kazakhstan University (Petropavlovsk, Kazakhstan), e-mail: asolodovnik@ku.edu.kz

Kleksin Roman is a Laboratory assistant at the M. Kozybayev North Kazakhstan University (Petropavlovsk, Kazakhstan), e-mail: fjolkunnigr@yandex.kz

Leontyev Pavel, Candidate of Physico-Mathematical Sciences is an Associate professor at the M. Kozybayev North Kazakhstan University (Petropavlovsk, Kazakhstan), e-mail: pleontyev@mail.ru, pleontiev@ku.edu.kz

Useinov Beibut, Candidate of Physico-Mathematical Sciences is a Professor at the M. Kozybayev North Kazakhstan University (Petropavlovsk, Kazakhstan) e-mail: buseinov@gmail.com

Markova Agniya is a Senior lecturer at the M. Kozybayev North Kazakhstan University (Petropavlovsk, Kazakhstan), e-mail: agni.m@bk.ru

Kassimova Svetlana is a Senior lecturer at the M. Kozybayev North Kazakhstan University (Petropavlovsk, Kazakhstan), e-mail: kassedy_sa@mail.ru